

# Numerical simulations on the aerodynamics of the Ahmed body at different slant angles

Gaurav Kumar<sup>1</sup>, Chanfiou Ahmed Mboreha<sup>2</sup> & Yahya Al-fakih<sup>3</sup>

<sup>1</sup>Department of Mechanical Engineering, Delhi Technological University, Delhi, India

Email: [gauravdtu@hotmail.com](mailto:gauravdtu@hotmail.com)

<sup>2</sup>Department of Aeronautical Engineering, Nanjing University of Aeronautics and Astronautics, Jiangsu, Nanjing, China,

Email: [chanfiou2017@nuaa.edu.cn](mailto:chanfiou2017@nuaa.edu.cn)

<sup>3</sup>Department of Mechanical Engineering and Automation, Northeastern University, Shenyang, Liaoning, China, Email: [engg.yahya@yahoo.com](mailto:engg.yahya@yahoo.com)

**Abstract:** In this research, the aerodynamic behavior of Ahmed's body with slant angles of  $0^\circ$ ,  $30^\circ$  and  $60^\circ$  is studied using ANSYS FLUENT CFD code. The flow conditions for all cases were same while the rear slant angle is varied for Ahmed's body. The aerodynamic parameters; lift coefficient and drag coefficient were focused mainly to analyze the flow behavior, it tells the aerodynamics efficiency. The time dependent transient simulation is run to study the behavior of fluid flow. As the Reynold's number lied  $5 \times 10^5$  in turbulent regime so to accurately capture the turbulent effects, k-epsilon two equation model with  $Y^+$  equal 50 is used. The results of velocity contour, pressure contour, Kinetic Turbulent Energy, velocity vector and velocity profile plots were presented and discussed in detail. The fluid flow behavior illustration of flow separation at rear region of Ahmed's body is captured by defining wake region domain. The results showed that by varying slant angle from  $0^\circ$  to  $30^\circ$  the flow is attached at rear slant region and flow separation is reduced but lift coefficient and drag coefficient values are increased by 4%, and 7% respectively. Whereas increasing the slant angle up to  $60^\circ$ , flow again detached the flow at rear region causing flow separation but there is not much difference in lift and drag coefficients as comparing to  $0^\circ$  slant angle configuration.

**Keywords:** Ahmed Body, CFD of Ahmed body, numerical solution, separation bubble, C-pillar vortex

## Nomenclature:

- |                           |                                  |
|---------------------------|----------------------------------|
| • $\phi/\theta$ (degrees) | Slant Angle                      |
| • S(dimensionless)        | Strouhal Number                  |
| • n(Dimensionless)        | Frequency of vortex shedding     |
| • $D_h$ (m)               | Hydraulic diameter of the shape  |
| • V(m/s)                  | Fluid velocity at Re             |
| • Re(Dimensionless)       | Reynolds number                  |
| • P(kg/m <sup>3</sup> )   | Air density                      |
| • $\mu$ (kg/m.s)          | Dynamics Viscosity of the air    |
| • L(m)                    | Characteristics linear dimension |

## I. INTRODUCTION

Fuel consumption is one of most important parameters that are directly related to aerodynamics efficiency of a vehicle [1]. The vehicle efficiency is to be maintained while achieving reduction in fuel

consumption by improving external car aerodynamic, CO<sub>2</sub> emissions and noise. Steady increase in power of computers is elevating simulating importance of the vehicle's external aerodynamics and calculating the corresponding characteristic numbers of aerodynamic. A significant part of the growth age of cars is consequently optimization invested. This is achievable particularly and only by development virtually. To create such car industry development processes, a reliable model for simulation validated by fundamental experiments [2].

The experimental studies provide the validated data to make use of bodies of models with characterized geometries by multiple restrictions, such as the back-slant angle. Ahmed body is an example for one such body, a bluff simple shaped body model with basic vehicle aerodynamic properties which is used for multiple investigations reference. The first measurement studied effect of slant angle in range from 0° to 40° at a velocity of flow at 40 m/s ( $Re = 5 \times 10^6$ ) by varying geometry slightly, also called Morel body [3]. The generic Ahmed Body reference model has been chosen as the benchmark for carrying out computations for studying of the aerodynamic parameters. The body was first proposed by Ahmed et al. [4] as can be seen in figure 1, Ahmed et al. conducted measurements under similar boundary conditions, which is called as Ahmed body nowadays. Later, drag forces and surface pressures were determined at full Reynold's number scale by Bayraktar[5]. They used model with geometric size 4.6 times bigger than the Ahmed body original size. Another study on flow behavior of Ahmed body was conducted by Lienhart[6] for measurements on velocity, turbulence, and pressure distribution properties of flow. The objective of that study was to experimentally investigate the Ahmed's body aerodynamic behavior under with different geometrical models and to investigate the CFD analysis using fluent package to compare with experimental information.

An excellent review of different approaches to modeling turbulence for bluff body simulations was given in said research (see references therein) in which it is discussed the use of Reynolds Averaged Navier Stokes (RANS) models, and three more alternatives to be combined with LES simulations: detached eddy simulation (DES), subgrid scale (SGS) models or the more general implicit LES (ILES) method [7].

The body represents the fundamental behavior of aerodynamics of a vehicle, rear part especially. The slant angle  $\phi$  has a high impact on the aerodynamic lift and drag at the rear part. Both coefficients of lift and drag change slightly at the angle  $\phi=30^\circ$  when moved from  $\phi=0$ . Thus, it is named as critical slant angle

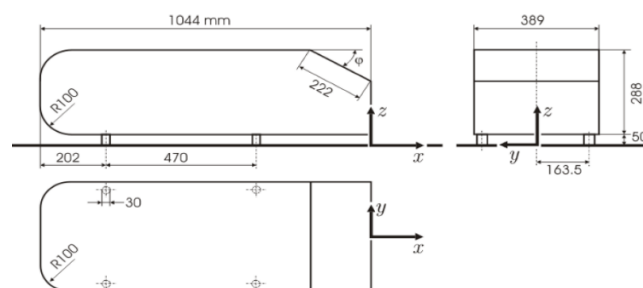


Figure 1: Ahmed's body dimensions sample [8]

In the automotive industry the simulation of 3D CFD flows through the vehicle is an essential tool for understanding the flow phenomenon for aerodynamics design. The flow behavior to the drag force of the body is complex phenomenon to be captured by turbulent models. Some important features of the

flow contributing in the fluid flow is ground flow of the Ahmed body and the separation of the flow from the vehicle, which is essential to be captured for the accuracy of the drag predictions [9].

## II. METHODOLOGY

### A. CFD Flow chart

The CFD process flowchart for the analysis of Ahmed's body is shown below:

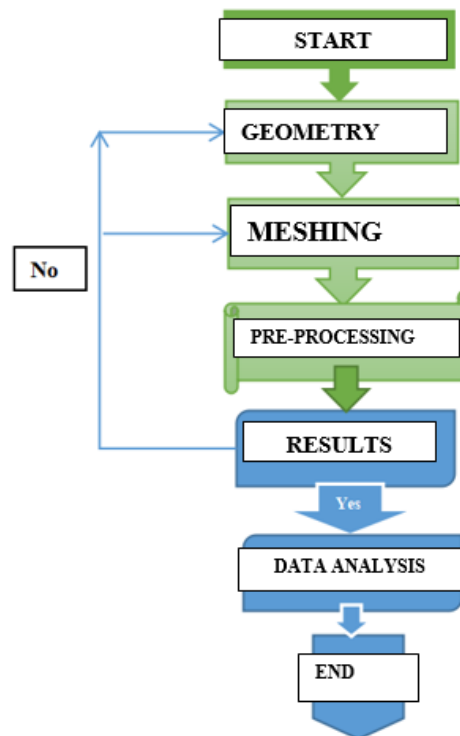


Figure 2: Flow-chart

### B. Mathematical Formulations:

The mathematical equations that has been used in this report are listed below

#### i. *Pythagorean Theorem:*

The Pythagorean Theorem was applied to find sides length of Ahmed body using the available angles and vice versa as given in equation (1). This theorem is applicable to find length of one side by using the other two lengths of the right-angle triangle as given in equation (2) and illustrated in figure (3):

Equation 1: Pythagorean Theorem Formula for angles.

$$\theta = \sin^{-1}\left(\frac{\text{opposite}}{\text{Hypotenuse}}\right)$$

Equation 2: Pythagorean Theorem Formula for side length.

$$(\text{Hypotenuse})^2 = (\text{opposite})^2 + (\text{Adjacent})^2$$

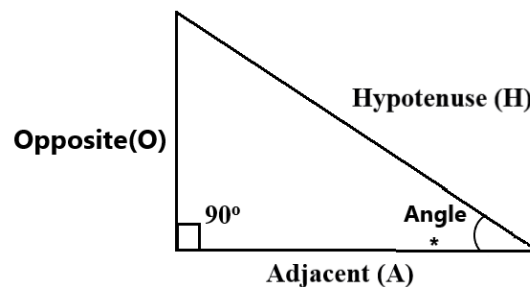


Figure 3: Illustration of Pythagorean Theorem on a triangle.

Area of Rectangle:

The formula to obtain area of rectangle by multiplication of length to width as given in equation (3)

$$A=LW; A=\text{Area}, L=\text{Length}, W=\text{width} \dots\dots(3)$$

ii. *Frequency of shedding:*

The frequency of shedding formula as given in equation (4).

$$S = \frac{nD}{v} \dots\dots(4)$$

iii. *Vortex shedding period:*

The formula to find the vortex shedding period as given in equation (5)

$$T = \frac{1}{n} \dots(5)$$

iv. *Reynolds number:*

The formulation to obtain the Reynolds number is given in equation (6) as it signifies the flow field behavior whether it is laminar or turbulent.

$$Re = \frac{\rho V L}{\mu} \dots\dots(6)$$

v. *3D Hydraulic diameter for Rectangle:*

The mathematical formulation to find hydraulic diameter for rectangle is given in equation (7)

$$D_h = \frac{2 \times \text{length} \times \text{height}}{\text{Length} + \text{height}} \dots\dots(7)$$

### C. Geometry of Ahmed's body:

For defining slant angles on Ahmed's body to create 30° and 60° slant angles at back surface, Chamfer button was selected to create this sharp edge. As those two cases are different in their angles, this step had different right and left length sides values. For determining those values for each of slant angle cases, two mathematical equations are used: equation (1) and (2). Ahmed's body shapes with three different angles (0°, 30°, 60°) are presented in figure 4

For 30° angle:

$$30 = \sin^{-1} \left( \frac{\text{Right length}}{222} \right) \rightarrow \text{Right length} = 111 \text{ mm}$$

$$(222)^2 = (111)^2 + (\text{Left length})^2 \rightarrow \text{Left length} = 192.26 \text{ mm}$$

For 60° angle:

$$60 = \sin^{-1} \left( \frac{\text{Right length}}{222} \right) \rightarrow \text{Right length} = 192.26 \text{ mm}$$

$$(222)^2 = (192.26)^2 + (\text{Left length})^2 \rightarrow \text{Left length} = 111 \text{ mm}$$

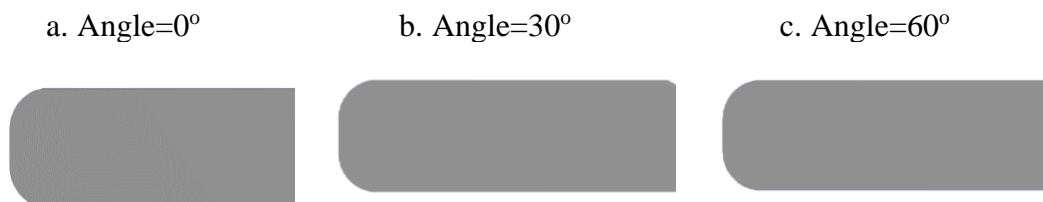


Figure 4: Ahmed's body shapes with three different angles (0°, 30°, 60°)

### D. Meshing generation and Boundary conditions in the three cases

#### i. Meshing generation

The most important part of CFD simulation is the mesh generation, as the results of CFD parameters: specific pressure and stress are calculated on these mesh cells defined by meshing. The division of the domain into small elements is done to simulate CFD solution with good convergence. The following steps were adopted for mesh generation, firstly the Reynolds number ( $5 \times 10^5$ ) is utilized to measure the flux velocity that is  $25.363 \text{ m/s}$ . For defining inflation layer thickness layers on Ahmed's body,  $Y^+$  method is used to define inflation layer thickness values for capturing wall effects near Ahmed's body surfaces. By knowing that the value of  $Y^+$  close to 30 is more desirable for wall functions so  $y^+$  has been taken to be 50 for getting more accurate results with all the air properties.

There are three refinement regions in Ahmed's body cases as defined below and as shown in figure 5:

First region – Transition from far-field to near field. Second region – Underbody of the body. Third region – Wake region

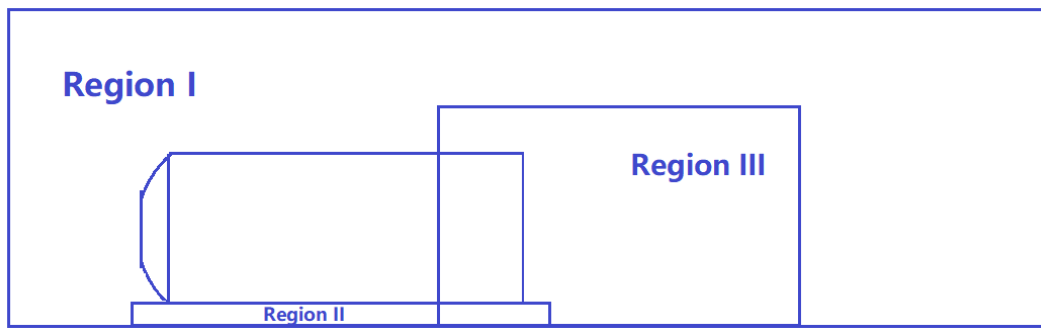


Figure 5: Regions mesh refinements.

ii. Results of the meshing parameters and mesh distribution:

The mesh generated on whole body is visualized here, the meshing parameters and distribution are quite refined and are reliable as compared with external sources. The mesh results are shown in figure .

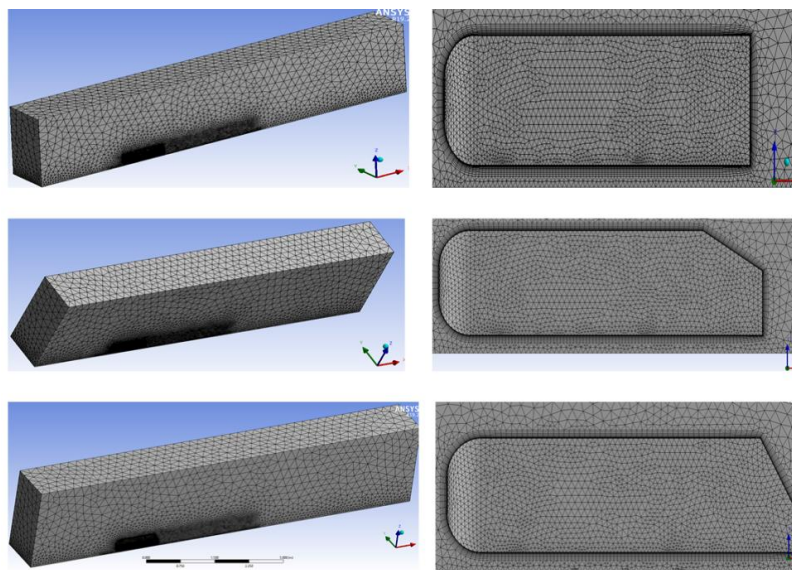


Figure 6: End of meshing of domain and Ahmed's body at 0°, 30° and 60°

iii. Boundary conditions in the three cases

All boundary conditions in the three cases are illustrated in the figure 7.

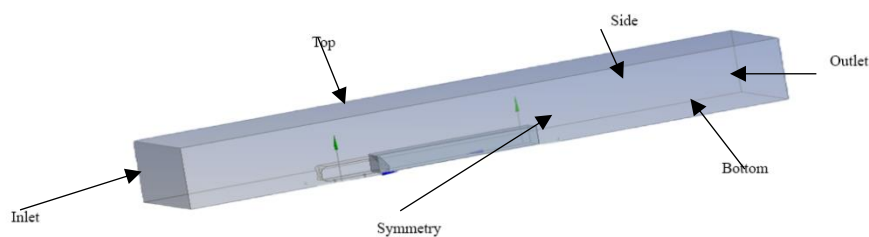


Figure 7: Boundary conditions in the three cases of Ahmed's body.

Table 1: Summary of the Mesh Parameters and mesh distribution

Parameter	Ahmed's body at 0° slant angle	Ahmed's body at 30° slant angle	Ahmed's body at 60° slant angle
Number of elements	555029	547085	553100
Number of nodes	156289	145666	155102
Element size	0.2 m	0.2 m	0.2 m
First layer height	0.00064 m	0.00064 m	0.00064 m
Maximum layers	12	11	11

#### E. Numerical Method:

The mesh has been transferred to FLUENT setup for defining boundary conditions and pre-processing for solving the three cases of Ahmed's body. The transient flow simulation is conducted for all three cases of Ahmed's body CFD analysis using pressure-based solver and the effects of gravity are taken in consideration. In the derivation of the k – epsilon model, the assumption is that the flow is fully turbulent, and the effects of molecular viscosity are negligible. The standard k –epsilon model is therefore valid only for fully turbulent flow[10]. The pressure-based solver along with SIMPLE algorithm is adopted under solution schemes. For the turbulent kinetic energy specific dissipation rate, momentum and pressure equations, 2<sup>nd</sup> order upwind discretization is selected. The gradient calculation from least square cell based is chosen. The solution solver setup with solver schemes are tabulated below for all the slant angles configurations of Ahmed's body. Here, we used reference area value as 0.11205 m<sup>2</sup> and velocity of air is 25.363 m/s with Pressure based solver is used because Mach number is low hence we can assume flow as incompressible and as due to capture flow at time intervals transient case is preferred.

Calculations that have been done in table 4:

Physical properties of Air that has been used are shown in table 5, these assumptions were considered for CFD analysis:

1. The surface of the Ahmed body was modeled using walls with no-slip.
2. The condition of the flow did not involve the temperature or the energy equation.
3. Incompressible flow.

Table 2: Air properties used in simulation.

Parameters	Values
Density	1.225 Kg/m <sup>3</sup>
Viscosity	1.7894x10 <sup>-5</sup> kg/m s
Ratio of specific heat	1.4
Temperature	288.16 K

At Re=5x 10<sup>5</sup>:

By known that the linear dimension = 0.288 m, the Velocity can be calculated by using the equation below:

$$Re = \frac{\rho V L}{\mu} \rightarrow 5 \times 10^5 = \frac{1.225 \times V \times 0.288}{1.7894 \times 10^{-5}} \rightarrow V = 25.35998 \frac{m}{s}$$

The  $D_h$  for Ahmed's body inlet can be determined from the equation 7:

$$D_h = \frac{2 \times length \times height}{Length + height} = \frac{2 \times 0.389 \times 0.288}{0.389 + 0.288} = 0.331 \text{ m}$$

1. From S vs. Re chart:

$$S \approx 0.2 \text{ At } Re = 5 \times 10^5$$

2. Frequency of shedding:

By knowing that the velocity is 25.363 m/s at  $Re = 5 \times 10^5$  and  $D_h = 0.331 \text{ m}$ , Frequency of vortex shedding can be calculated using equation 4:

$$S = \frac{n D}{V} \rightarrow n = \frac{25.363 \times 0.2}{0.331}$$

$$n = 15.325$$

3. Vortex shedding period:

By knowing the value of Frequency of vortex shedding, period can be calculated using equation 5:

$$T = \frac{1}{n} = \frac{1}{15.32507} = 0.0653 \text{ s}$$

4. Time step size:

By break the period into 50 pieces

$$\Delta T = \frac{\text{Vortex shedding period}}{50} = \frac{0.0653}{50} \approx 0.001306$$

5. Number of time steps:

$$N = \frac{\text{Total time for 20 period}}{\text{Time step size}} = \frac{0.0653 \times 20}{0.001306} \approx 1000$$

6. Area of the Ahmed's body inlet

$$\text{Area} = \text{Length} \times \text{Width} = 0.389 \times 0.288 = 0.112032 \text{ m}^2$$

### III. SIMULATION OUTCOMES

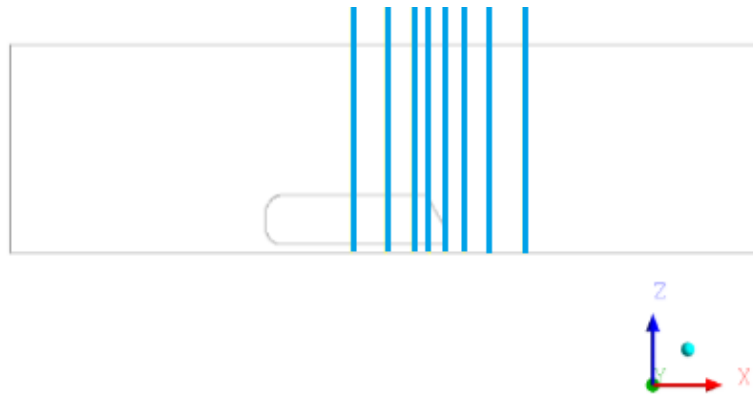


Figure 8: Illustrating the location of the lines on Ahmed's body for creating velocity profile

As the CFD simulation of Ahmed’s body is completed at defined inputs and convergence criteria so the results are obtained using post processing through CFD Post. The velocity contours, velocity vector, pressure contours and turbulence kinetic energy contours are obtained as results to analyze the performance of Ahmed’s body. At the end (Insert → Location → Line) was selected to create the velocity profile charts for each of the slant angle Ahmed’s body case. The following steps in table (6) has been followed for all the slant angles cases in order to capture the flow over at the rear side of the Ahmed’s body and monitor lines to be formed in two positions as illustrated in figure (8).

Table 3: Inserting lines to create velocity profile for all slant angles.

Line 1			
Point 1	-0.544	0	1.5
Point 2	-0.544	0	0
Line 2			
Point 1	-0.344	0	1.5
Point 2	-0.344	0	0
Line 3			
Point 1	-0.194	0	1.5
Point 2	-0.194	0	0
Line 4			
Point 1	-0.094	0	1.5
Point 2	-0.094	0	0
Line 5			
Point 1	0	0	1.5
Point 2	0	0	0
Line 6			
Point 1	0.106	0	1.5
Point 2	0.106	0	0
Line 7			
Point 1	0.256	0	1.5
Point 2	0.256	0	0

Line 8			
Point 1	0.456	0	1.5
Point 2	0.456	0	0

A. Lift coefficient and Drag coefficient profiles for the three cases of Ahmed’s body.

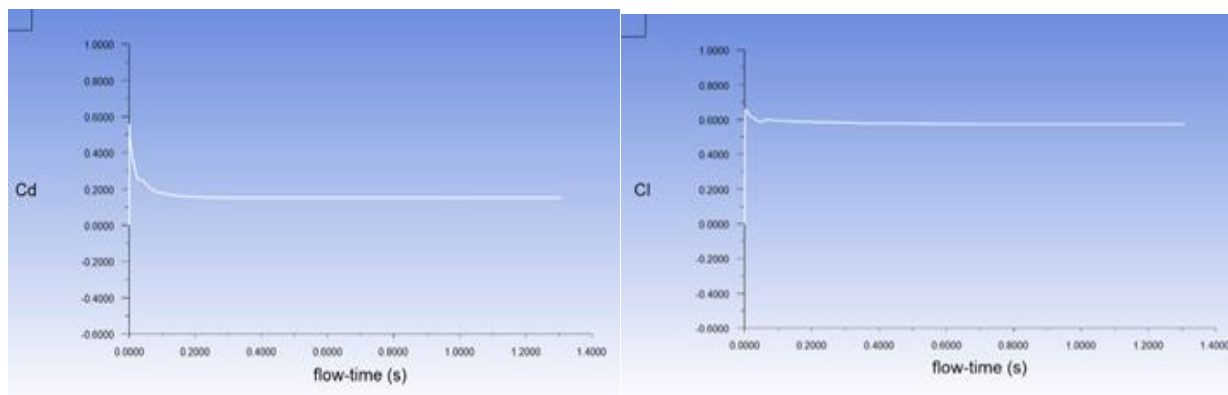


Figure 9: Lift coefficient (Right) and Drag coefficient (left) for 0° slant angle

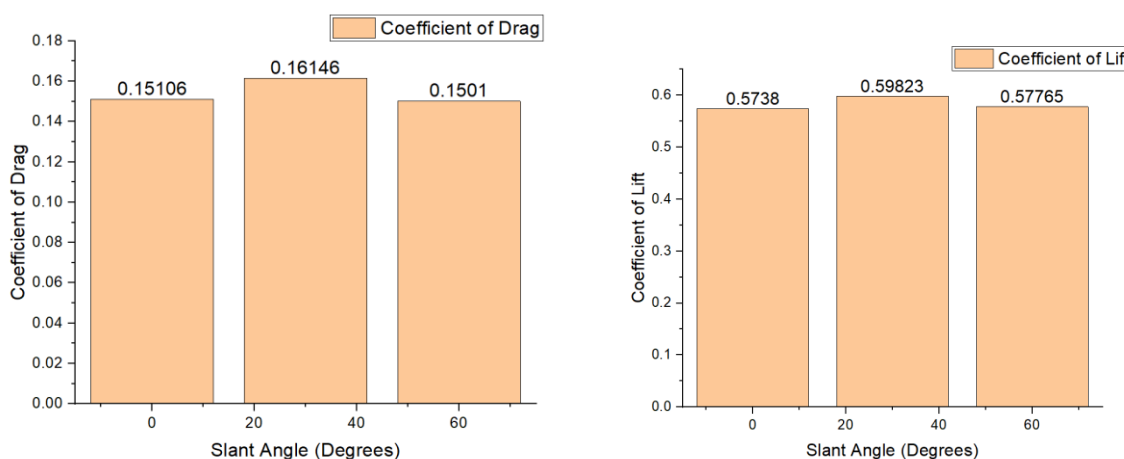


Figure 10: Coefficient of Drag vs Slant Angle & Coefficient of Lift vs slant angle

i. Lift coefficient and Drag coefficient for 0° slant angle:

Lift coefficient and Drag coefficient plots illustrated that the drag and the lift values converged to 0.15016 for Cd and 0.57380 for Cl for Ahmed's body with 0° slant angle as shown in figure 9. The lift coefficient and drag coefficient profiles are showing straight line while converging to final iteration shows that values of lift coefficient and drag coefficient are quite accurate for defined flow condition.

i. Lift coefficient and Drag coefficient plot for 30° slant angle:

Lift coefficient and Drag coefficient plots illustrated that the drag and the lift values converged to 0.16146 for Cd and 0.59823 for Cl for Ahmed's body with 30° slant angle as can be seen in figure 11. The lift coefficient and drag coefficient plots are showing straight line while converging to final

iteration shows that values of lift coefficient and drag coefficient are quite accurate for defined flow conditions.

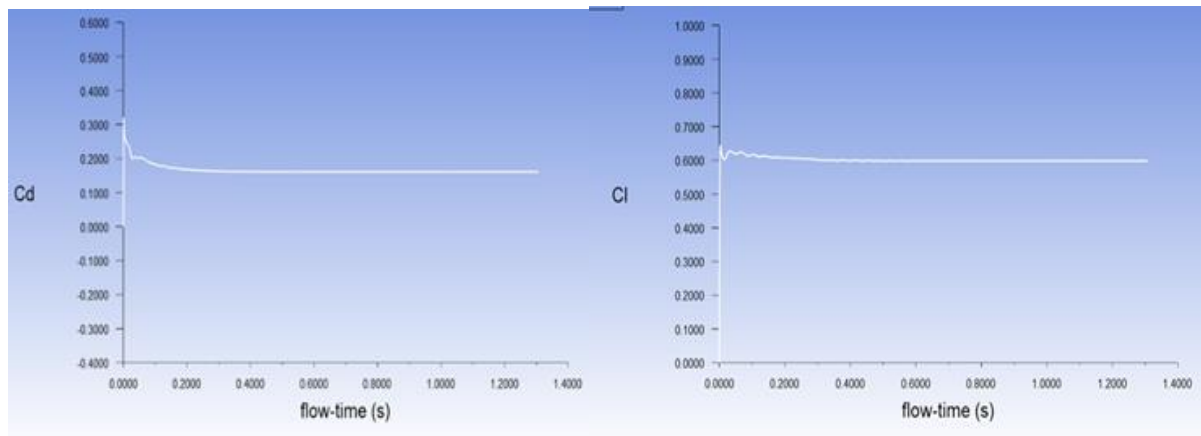


Figure 11: Lift coefficient (Right) and Drag coefficient (left) for 30° slant angle

ii. *Lift coefficient and Drag coefficient for 60° slant angle:*

Lift coefficient and Drag coefficient plots illustrated that the drag and the lift values converged to 0.15010 for Cd and 0.57763 for Cl for Ahmed's body with 6° slant angle as shown in figure 12. The lift coefficient and drag coefficient plots are showing straight line while converging to final iteration shows that values of lift coefficient and drag coefficient are quite accurate for defined flow conditions.

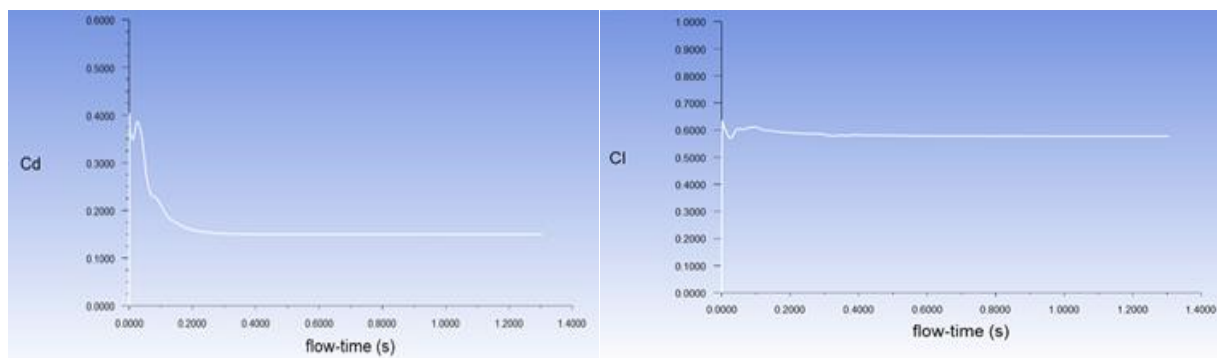


Figure 12: Lift coefficient (Right) and Drag coefficient (left) for 60° slant angle

B. *Velocity contour and Turbulence Kinetic Energy plots for the three cases of Ahmed's body (0°, 30° and 60° slant angles):*

The contour colors variation is showing change in velocity. The maximum velocity in 0° slant angle case is 63.23 m/s which is almost same as 60° slant angle case which shows 62.30 m/s but for 30° slant angle, it shows 59.17 m/s. As expected, the highest value occurs top surface of Ahmed's body as the frontal curvature increase to smooth top surface increases velocity as the pressure drag is less on top surface. The nose of the shape has almost zero velocity value as the flow is striking on frontal face and causing pressure drag and has very low velocity at the rear slant side due to formation of vortices. The green area agrees with the velocity value which is 25.363 m/s, while blue area shows low velocity and

high-pressure region and red area gives high velocity and low-pressure region. Where the pressure is low the velocity increases and where pressure is high the value of velocity decreases. The velocity contours showed that with increase in slant angle up to  $30^\circ$ , the flow nearly attached to slant surface in the wake region, and the form drag consequently decreases as the rear slant angle increased from  $0^\circ$  slant angle to  $30^\circ$  slant angle. As the slant angle is increased to  $60^\circ$  the flow is again separated at rear region and flow vortices are significant. The value of lift coefficient and drag coefficient is increased as the slant angle is increased from  $0^\circ$  to  $30^\circ$  as the flow is more attached to surface whereas the slant angle is further increased to  $60^\circ$  the flow separation increases at slant region causing decrease in lift coefficient

When flow becomes turbulent, transport mechanisms like diffusion highly increases beyond the molecular diffusion. For the deviation in slant angles, figure (13) illustrate the thickness of these streams which is determined by turbulent kinetic energy where the flow is separated and in coincidence of the lower horseshoe vortex in  $30^\circ$  slant angle case and wider vortex in  $60^\circ$  slant angle case but still in  $30^\circ$  slant angle case has the wider shape of vortex as flow is more attached to body at slant. The wake region has shown the same results as the velocity contours and that's can be explained as the Kinetic energy is directly proportional to velocity.

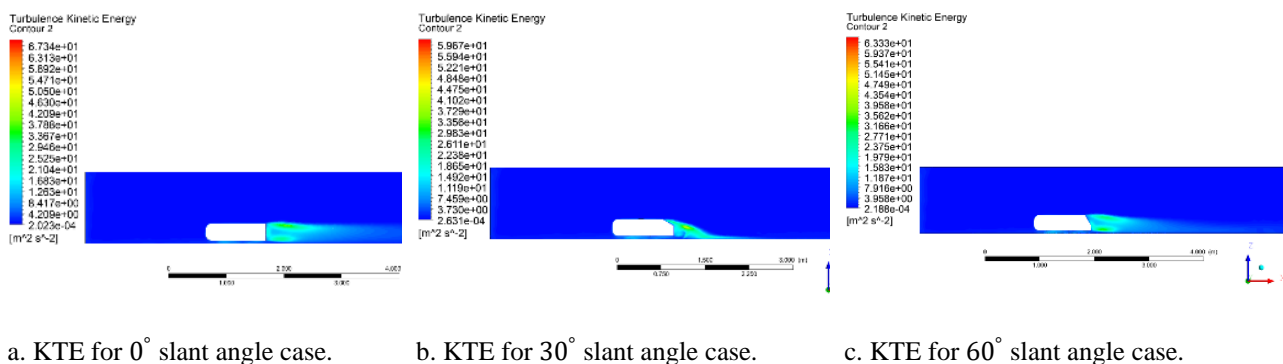


Figure 13: Turbulence Kinetic Energy for the three cases of slant angles.

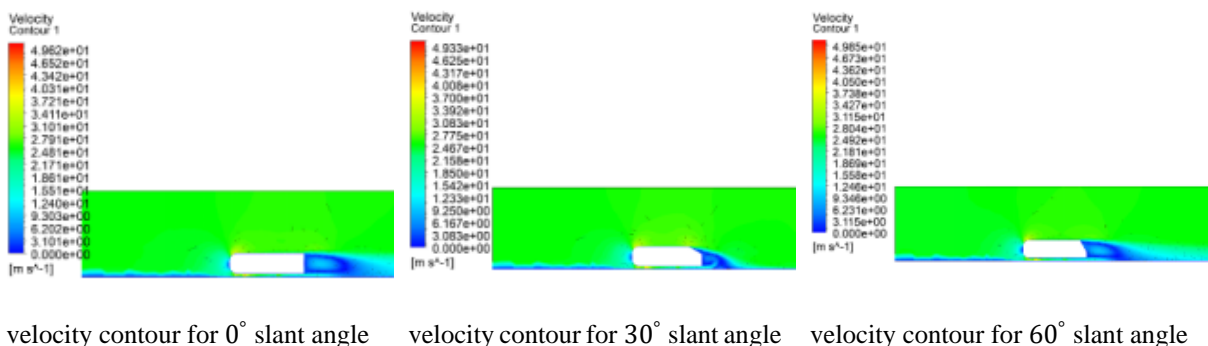
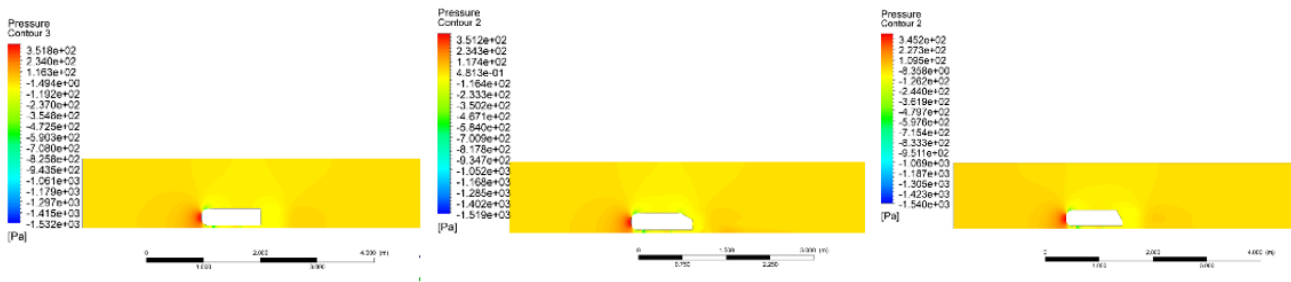


Figure 14: Velocity contours for the three cases of slant angles.

C. Pressure plots for the three cases of Ahmed's body ( $0^\circ$ ,  $30^\circ$  and  $60^\circ$  slant angles):



**a. Pressure contour for 0° slant angle    b. Pressure contour for 30° slant angle    c. Pressure contour for 60° slant angle**

Figure 15: Pressure contours for the three cases of slant angles.

As the air strikes the frontal area of vehicle, velocity is reduced at frontal face as very high pressure of air acts on the vehicle’s front engine’s grill which is highlighted in red coloured contour.

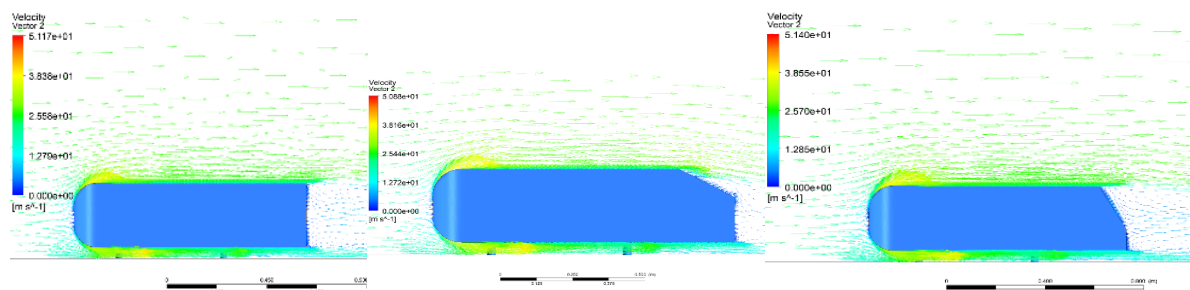
Further, the flow of air gets separated between lower and upper vehicle surfaces. As the air travels over the curved nose surface of Ahmed body, it accelerates with high speed on surface that is forward-facing, causing a drop-in pressure. This low-pressure creates lift over the surface of the roof and the pressure on bottom of vehicle as the air pass on it.

A notch is formed by the back slant owing to separation of flow as the air continue to flow and to the back, leaving a space of low pressure or vacuum where the air won’t be able to properly fill as can be seen in figure (15).

**D. Velocity vector plots for the three cases of Ahmed’s body (0°, 30° and 60° slant angles):**

The velocity vector contour shows that the air starts to separate when it strikes with Ahmed’s body showing velocity reduces significantly at the frontal region thus it can be expressed that maximum pressure occurs in this region as can be seen in figure (16).

Further, the velocity vectors move along the curves of the shape so that their values increased and then it separated to flow around the body in both sides. The velocity decreases at rear slant region minimum as flow separation occurs that results in to vortices. The vortices change in its width from one case to another and also in its intensity as 0° slant angle case shows the highest intensity and wider vortices than the other cases as shown in figure.



a. Velocity vector for 0° slant angle case    b. Velocity vector for 30° slant angle case    c. Velocity vector for 60° slant angle case

Figure 16: Velocity vector plots for the three cases of Ahmed's body.

E. Velocity profiles plots referring to Z axis, for the three cases of Ahmed's body (0°, 30° and 60° slant angles):

The flow over the rear side of Ahmed's body is captured as velocity profiles with the use of lines inserted on rear side of body. The velocity profiles are shown in figure 17, figures (a, b and c) illustrate the flow behavior affected by slant angles in Ahmed's body.

These plots start just before the slant region of Ahmed's body showing the velocity before facing the slant angle and then velocity changes abruptly as it passes the slant region. The change in velocity is nearly same for slant angles of 0° and 60° but for 30° slant angle, it shows significant fluctuation in velocity comparing to other two slant angles and that's prove why the drag coefficient and lift coefficient values in this case are higher than the other two cases .

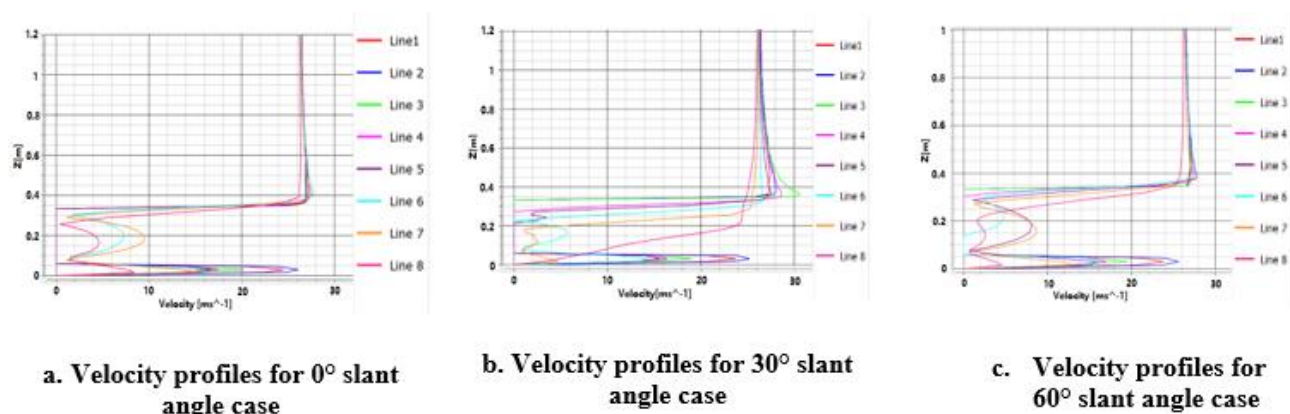


Figure 17: Velocity profiles for 0°, 30° and 60° slant angles cases.

#### IV. DISCUSSION

The CFD results obtained the velocity contours, velocity vectors, pressure contours and turbulent kinetic energy contours. It has been known that airflow velocity is inversely proportional to the pressure to keep the algebraic sum of potential energy, kinetic energy, and pressure constant. The high pressure at frontal face of Ahmed's body resulted as the air flow strikes perpendicularly at front face, the air velocity decreases as the result of increase in pressure at frontal region. The air flow continues to flow on upper curved path of Ahmed's body, this curvature provides a way to accelerate the flow on upper surface. Similarly flow passes through bottom surface of Ahmed's body but the flow velocity is less as compared to top surface. This velocity difference of top and bottom surfaces of Ahmed's body causes decrease in pressure at top surface and increase in pressure at lower surface resulting into lift generation. Further, the flow moves toward the rear slant angle in each case and it started to separate forming vortices with high intensity as it's a turbulent flow, but still the vortices strength varied from one case to another as Ahmed's body shape with 0° slant angle shows wider vortices than 30° as flow becomes attached at rear region but when 60° slant angle is studied, it showed that vortex strength is increased again due to flow separation at slant side. The velocity contours results showed that for different slant angles the flow behavior varies at rear region of Ahmed's body. The results illustrated

that with increase in slant angle up to  $30^\circ$ , the flow is nearly attached to slant surface in the wake region, and the form drag consequently decreases as the rear slant angle is increased from  $0^\circ$  slant angle to  $30^\circ$  slant angle. When the slant angle is further increased to  $60^\circ$  the flow is again separated at rear region and flow vortices are significant. The value of lift coefficient and drag coefficient is increased as the slant angle is increased from  $0^\circ$  to  $30^\circ$  as the flow is more attached to surface whereas the slant angle is further increased to  $60^\circ$  the flow separation increases at slant region causing decrease in lift coefficient. This shows that flow is more attached to Ahmed’s body with  $30^\circ$  slant angle configuration. For the difference in slant angles, it is obvious that at the initial section of the rear slant, the pressure increases (evident by the decreasing green area) with decreasing value of rear slant angle from  $30^\circ$  to  $0^\circ$ . This is due to less dramatic change in the direction of airflow, resulting in decreased notch formation (vacuum region or low pressure). This results in more steady pressure between the top and bottom surfaces of the Ahmed body and hence, reduced tendency of lift. The results showed that lift coefficient and drag coefficient increased with increase in rear slant angle from  $0^\circ$  slant angle to  $30^\circ$  slant angle because of the larger pressure difference happened between bottom and top surfaces of the Ahmed’s body. On the other hand, the both the drag coefficient and lift coefficient decreased by increasing rear slant angle is increased from  $30^\circ$  slant angle to  $60^\circ$  slant angle as the flow is again detached at rear slant region causing flow separation resulting in loss of lift. Shape effects on drag are presented in figure (18).

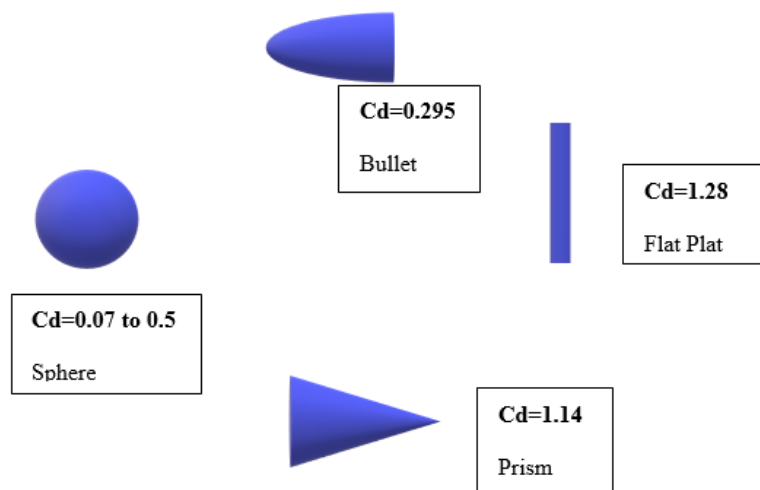


Figure 18: Shape effects on Drag

In figure (18), we can easily see that at same frontal area, then,  $C_d$  is depends upon only shape

From the observations, we found that at  $30^\circ$  slant angle, value of  $C_d$  is very high as comparison to other two slant angles like  $60^\circ$  and  $0^\circ$ . Hence,  $30^\circ$  is not a suitable choice as it will consume more fuel and not so efficient.

Table 4: Lift and Drag coefficient convergence for flow past Ahmed's body cases.

Slant Angles	$C_d$	$C_L$
$\theta=0^\circ$	0.15106	0.57380

$\theta=30^\circ$	0.16146	0.59823
$\theta=60^\circ$	0.15010	0.57765

We can see drag and lift is maximum at 30-degree slant angles as comparison to other slant angles case. This is occurring due to couple of vortices developed, and the flow leave the body at the lower edge of the slant. This leads to very strong under pressures at that position, so that the coefficient of drag reaches its maximum in this position at angle  $=30^\circ$ . The difference between lift coefficient and drag coefficient values of Ahmed's body configurations of  $0^\circ$  slant angle to  $30^\circ$  slant angle. Whereas for the  $60^\circ$  slant angle configuration the lift coefficient is increased to 7 percent and drag coefficient is increased to 4 percent as compared to  $0^\circ$  slant angle configuration.

## V. CONCLUSION

The CFD analysis of Ahmed's body with slant angles of  $0^\circ$ ,  $30^\circ$  and  $60^\circ$  is studied using ANSYS FLUENT with same fluid flow conditions. The Design Modeler tool of ANSYS is used for CAD model preparation of Ahmed's body different cases. As the Reynold's number lied in turbulent k-epsilon two equation turbulent model is used with transient flow analysis. The results of velocity contour, pressure contour, Kinetic Turbulent Energy, velocity vector and velocity profile plots are presented for analysis of aerodynamic behavior of Ahmed's body. The results showed that by varying slant angle from  $0^\circ$  to  $30^\circ$  the flow is attached at rear slant region and flow separation is reduced but lift coefficient and drag coefficient values are increased. Whereas increasing the slant angle to  $60^\circ$ , flow again detached the flow at rear region causing flow separation but there is not much difference in lift and drag coefficients as comparing to  $0^\circ$  slant angle configuration. The following conclusions are drawn from results:

1. The minimum drag coefficient was 0.15010 is obtained in Ahmed's Body with  $60^\circ$  rear slant angle.
2. The minimum lift coefficient was 0.5738 is obtained in Ahmed's Body with  $0^\circ$  degree rear slant angle.
3. The lift coefficient and drag coefficient increased by 4%, and 7% respectively as increasing the slant angle from  $0^\circ$  to  $30^\circ$ . The boundary layer separation occurs on the rear slant caused increase in drag coefficient. However, Lift coefficient increased with increasing in rear slant angle due to larger pressure difference formed.
4. The flow separation vortices at rear region of wake area decreased with increase in slant angle up to  $30^\circ$ . This happened at rear end as a result of pressure difference, the flow on top and bottom of Ahmed's body joined at trailing region thus reducing drag causing vortices. As there are small vortices at back of Ahmed's body so less dissipation of kinetic energy takes place. The vehicle engine will require less power for propelling car in forward direction.
5. Wake is a region of recirculated flow which induces low pressure behind the car which is the main cause of the aerodynamic drag of car.

## VI. FUTURE SCOPE OF STUDIES

Here, we discussed about the effect of slant angles on the coefficient of drag & coefficient of lift. It is fully optimized but somehow, we can say other factors can also affect  $C_d$  drastically. Future researchers may work on the shape of the Ahmed body and other slant angles to see some more results at which slant angle, drag and lift is more.

**Conflict of interest:** The authors declare that they have no conflict of interest.

**Ethical statement:** The authors declare that they have followed ethical responsibilities

## REFERENCES

- [1] Zulfaa Mohamed-Kassim, Antonio Filippone, Fuel savings on a heavy vehicle via aerodynamic drag reduction, *Transportation Research Part D: Transport and Environment*, Volume 15, Issue 5, 2010, Pages 275-284, ISSN 1361-9209, doi.org/10.1016/j.trd.2010.02.010
- [2] Blazek, J. (2015). *Computational Fluid Dynamics: Principles and Applications: Third Edition*. In *Computational Fluid Dynamics: Principles and Applications: Third Edition*. doi.org/10.1016/C2013-0-19038-1
- [3] Costa, B. (2015). Studying the Airflow Over a Car Using an Ahmed Body. In *Comsol* (p. Page: 23.). [https://www.researchgate.net/publication/325451944\\_CFD\\_Study\\_of\\_Flow\\_over\\_a\\_Simplified\\_Car\\_Ahmed\\_Body\\_Using\\_Different\\_Turbulence\\_Models](https://www.researchgate.net/publication/325451944_CFD_Study_of_Flow_over_a_Simplified_Car_Ahmed_Body_Using_Different_Turbulence_Models)
- [4] Ahmed, S. R., Ramm, G., & Faltin, G. (1984). Some salient features of the time-averaged ground vehicle wake. *SAE Technical Papers*, Pages: 71\_77. doi.org/10.4271/840300
- [5] Bayraktar, I., Landman, D., & Baysal, O. (2001). Experimental and computational investigation of Ahmed body for ground vehicle aerodynamics. *SAE Technical Papers*, Page: 2\_3. doi.org/10.4271/2001-01-2742
- [6] Lienhart, H., & Becker, S. (2003). Flow and turbulence structure in the wake of a simplified car model. *SAE Technical Papers*, Page: 2\_3
- [7] Bello-Millán, F. J., Mäkelä, T., Parras, L., del Pino, C., & Ferrera, C. (2016). Experimental study on Ahmed's body drag coefficient for different yaw angles. *Journal of Wind Engineering and Industrial Aerodynamics*, 157, 140–144. doi:10.1016/j.jweia.2016.08.005
- [8] Hinterberger, C., M. García-Villalba, W. Rodi (2004) Large eddy simulation of flow around the Ahmed body. In: McCallen R, Browand F, Ross J (Eds.) *Lecture notes in applied and computational mechanics / The aerodynamics of heavy vehicles: trucks, busses, and trains*, Springer Verlag
- [9] Guilmineau, E. (2008). Computational study of flow around a simplified car body. *Journal of Wind Engineering and Industrial Aerodynamics*, 96(6–7), 1207\_1217. doi.org/10.1016/j.jweia.2007.06.041
- [10] Maheshkumar Maruti Patil, Mariappan D. Nadar, Suhas A. Uthale (2016) To investigate Heat Loss of a Fluid flowing through a Pipeline for Turbulent Flow. *International Journal of Advanced Engineering Research and Applications (IJAERA)*